Quantitative Characterization of Optical Coupling in Nanoporous ZnO-WO_3 and ZnO-PEDOT Composite Electrodeposited Gratings using Electrodiffraction Measurements

*Han Wai Millie Fung, Seulgi So, Kellen Kartub, and Robert M. Corn**

Department of Chemistry, University of California-Irvine, Irvine, CA 92697, USA.

Corresponding Author

*Robert M. Corn: rcorn@uci.edu

Abstract

In order to quantitatively characterize the optical coupling between ZnO (a high refractive index, but non-absorptive material) and an electrochromic material (either tungsten oxide (WO_3) or poly(3,4-ethylenedioxythiophene) (PEDOT)), electrodiffractive and electrochromic properties were investigated from a novel two-component composite nanostructured electrodeposited grating that incorporated both ZnO and either WO_3 or PEDOT. The sequential electrodeposition of these two materials through a photopatterned photoresist layer onto a fluorine-doped tin oxide (FTO) coated glass substrate created a grating structure that exhibited optical diffraction that could be modulated electrochemically. SEM images of the electrochromic gratings revealed that the ZnO electrodeposition created a high surface area nanostructured thin film. The nanostructured ZnO is non-absorbing, but its high refractive index and large surface area redirect light into the electrochromic grating and create a four-fold enhancement in the grating's electrodiffractive response.

Introduction

Zinc oxide's (ZnO) well-documented optical properties have been utilized for a variety of light-based applications. For example, its wide band gap (3.37 eV) has made ZnO a popular semiconductor material for photosensitized dyes with enhanced photovoltaic efficiency.[1-3] In addition to its semiconductor capabilities, ZnO has been observed to enhance the optical properties within various systems. ZnO was reported to improve the light trapping capabilities of solar cells both as a thin film on an absorbing material[4] and as a nanopatterned surface.[5-6] Within our lab, we observed that ZnO nanostructures used in a hierarchical fashion on Au and PEDOT nanocone array surfaces enhanced the antireflective properties of the nanocone arrays via optical coupling.[7] This is striking because while ZnO has no absorptive properties itself, it seemed to enhance those of the host material beneath. To further our understanding of the optical enhancement of ZnO, we extend our previous work on ZnO nanocone arrays and turn to optical diffraction gratings made of composite electrodeposited ZnO and electrochromic WO_3 or PEDOT in order to quantify the optical coupling effects.

Optical diffraction gratings that split, redirect, and disperse light are fundamental optical elements that have been incorporated into a myriad of optical devices including laser barcode scanners, optical switches, and spectrometers.[8-16] Their simple design only requires a surface or thin film material with an optical response that varies periodically on the order of the wavelength of light in order to exhibit optical diffraction. If we define the linear optical response in terms of the complex refractive index $n = \eta + i\kappa$, then periodic variations in κ are typically called absorptive gratings, while periodic variations in η are described as phase gratings.[17-23] Within our own system, ZnO is known to have a large η value (η = 1.998 at 633 nm), but no κ. Therefore we

theorize that any changes observed in κ in the presence of ZnO must be due to coupling of the ZnO with the absorptive components within the gratings.

In order to probe the absorptive effects (κ) in addition to the refractive effects (η) of our optical gratings, electrochromic materials were selected as an absorptive host material. Electrochromic thin films are a unique class of materials with a complex refractive index that can be varied reversibly by either oxidation or reduction reactions induced by changes in an applied potential in an electrochemical cell. The electrochromism of these thin films specifically refers to the electrochemically induced color changes. Considering that any changes to the absorptive properties of a material implies a change to the imaginary part of the refractive index, electrochromic thin films demonstrate a potential dependence of κ; however, changes in η, the real part of the complex refractive index, can also occur. Two of the most well-studied electrodeposited electrochromic thin film materials are tungsten oxide (WO_3)[24-27] and poly(3,4-ethylenedioxythiophene) (PEDOT).[28-32] Typical potential dependent variations of κ for these two materials are ±0.09 and ±0.07, respectively, in the visible region at 600 nm.[33-34] Due to the potential dependence of η and κ for electrochromic thin films, diffraction gratings that are fabricated from these materials also exhibit a diffraction efficiency that varies with applied potential. This effect has been observed previously and has been denoted as either "electrochemically modulated diffraction"[22, 35-37] or "electrotunable diffraction",[38-39] but in this paper, we will denote this phenomenon simply as "electrodiffraction."

In this article, we have observed and quantified the enhancement of electrodiffraction from a novel two-component composite nanostructured diffraction grating that incorporates both an electrochromic material (either WO_3 or PEDOT) and a nanostructured high refractive index ZnO (η = 1.998 at 633 nm). These composite gratings are fabricated by a two-step

electrodeposition process on a fluorine-doped tin oxide (FTO) coated glass substrate as depicted schematically in Figure 1. A pattern of 10 μm wide lines of either WO_3 or PEDOT separated by 5 μm of glass is created by electrodeposition onto an FTO glass substrate that is partially protected with a photopatterned film of photoresist. This initial electrochromic grating pattern has a film thickness of about 200 nm. A second electrodeposition step creates a nanostructured ZnO film on top of the electrochromic grating, with a film thickness of typically 600 nm. We show that this non-absorbing nanostructured ZnO film enhances both the optical absorption and the electrodiffraction from this grating; the optical coupling between ZnO and the electrochromic host material and results in a four-fold increase of the electrodiffractive response.

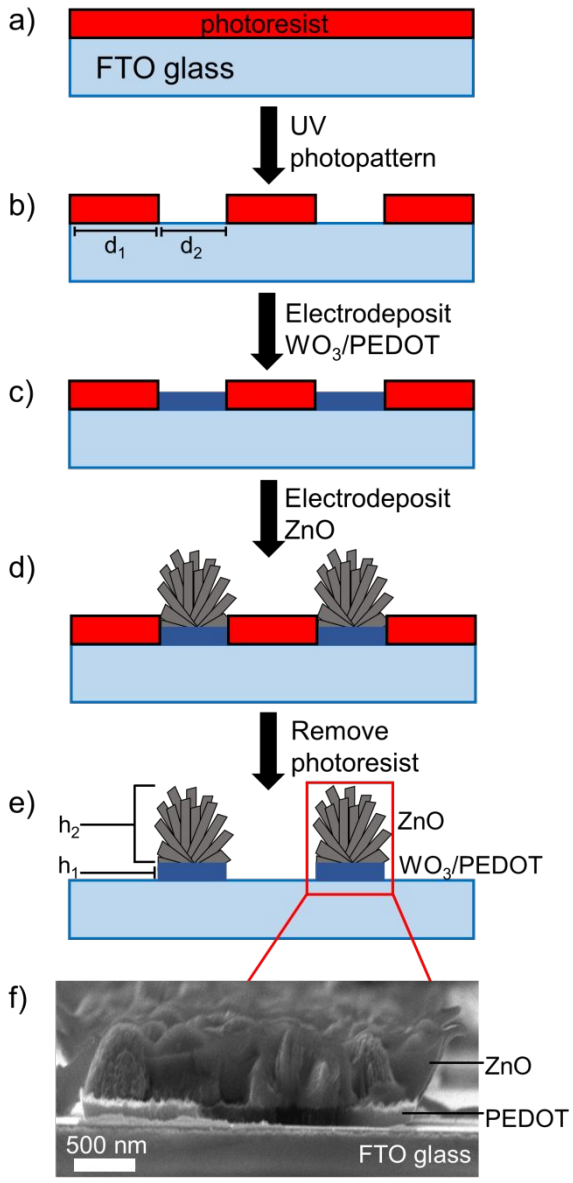

Figure 1. Schematic of the fabrication process of ZnO-WO_3 and ZnO-PEDOT gratings shown in a) – e). A cross-sectional SEM image f) reveals the various components of a sample ZnO-PEDOT grating.

Experimental Considerations

Fabrication of WO_3 gratings. FTO coated glass slides (~30 Ω/sq cm, Sigma-Aldrich) were cleaned by ultrasonication in an aqueous Hellmanex (1%) solution, rinsed with deionized water and ethanol, and dried under an N_2 stream. The FTO coated glass slides were then plasma cleaned under O_2 plasma for 2 min. S1808 positive photoresist was spincoated at 2500 rpm for 80 s onto the glass slides, baked at 90°C for 25 min to evaporate photoresist solvent, and cooled to room temperature. The photoresist coated glass slides were exposed to a UV lamp source (50 W, Oriel Instruments He(Xe) arc lamp) for 3.5 s and patterned using a photomask with 5 μm wide Cr lines and 10 μm glass spacings. The photoresist was then developed for 25 s using MF-319 developer (Microchem), rinsed with deionized water, and dried under an N_2 stream. An electrical contact area was made by dissolving the corner of the photoresist with acetone using a Q-tip. WO_3 was then electrochemically deposited onto the photopatterned FTO substrate using a potentiostat (PGSTAT12, Metrohm Autolab) in a three-electrode setup. The working electrode of the photopatterned FTO substrate was exposed to an aqueous peroxytungstatic acid ($H_2W_2O_{11}$) plating solution for 150 s at a cathodic potential of −0.5 V vs. a Ag/AgCl reference electrode in the presence of a Pt counter electrode.

Fabrication of PEDOT gratings. FTO glass slides (~30 Ω/sq cm, Sigma-Aldrich) were degreased by sonication in deionized water, acetone, and methanol, and then dried with a nitrogen jet. Poly(3,4-ethylenedioxythiophene)-poly(styrenesulfonate) (PEDOT:PSS, 2.0 wt. % in H_2O, Sigma-Aldrich) was mixed with isopropyl alcohol and ethylene glycol (ratio 85:10:5) to enhance electronic conductivity and improve wetting. A thin PEDOT:PSS layer was spincoated onto the FTO glass substrate at 3000 rpm for 20 s. Positive photoresist (S1808, Microchem) was then spincoated at 2500 rpm for 80 s onto the FTO glass substrate, and baked at 90°C for 25 min to evaporate the photoresist solvent. After cooling down to room temperature, the photomask

with 5 μm wide Cr lines and 10 μm glass spacings was placed flushed onto the substrate. The photoresist was exposed through the photomask using a UV lamp source (50 W, Oriel Instruments He(Xe) arc lamp) for 3.5 s. The photoresist was patterned and developed with MF-319 developer, rinsed with deionized water, and dried under a N_2 stream. An electrical contact area was made by dissolving the corner of the photoresist with acetone using a Q-tip. The PEDOT electrodeposition was performed with a potentiostat (PGSTAT12, Metrohm Autolab), where the FTO glass substrate was exposed to an aqueous electrolyte consisted with 0.02 M 3,4-ethylenedioxythiophene (EDOT, 97%, Sigma-Aldrich), 0.1 M sodium dodecyl sulfate (SDS) and 0.1 M lithium perchlorate ($LiClO_4$, 99.5%, Alfa), at a constant potential of +1.0 V vs. a Ag/AgCl reference electrode for 45 s in the presence of a Pt counter electrode.

Fabrication of nanostructured ZnO gratings. The electrodeposition of nanostructured ZnO was performed with a potentiostat (PGSTAT12, Metrohm Autolab) using a three-electrode setup. An aqueous solution containing 0.1 M $Zn(NO_3)_2$•$6H_2O$ (98%, Sigma-Aldrich) and 0.1 M KCl heated to 70°C was used as the plating solution. The working electrode of either a WO_3 or PEDOT grating array surface was exposed to the plating solution for 600 s at a constant potential of −0.9 V vs. a Ag/AgCl reference electrode and in the presence of a Pt counter electrode to form a nanostructured ZnO film over the WO_3 or PEDOT gratings. Finally, the sample was rinsed with acetone to remove remaining photoresist, and dried under a N_2 stream.

Morphological characterization. SEM images were obtained using a FEI Magellan 400 field-emission scanning electron microscope at an accelerating voltage of 5 kV. AFM measurements were collected using an Asylum Research MFP-3D, and AFM images were analyzed using Gwyddion imaging processing software. XPS measurements were collected using a Kratos Analytical AXIS Supra surface analysis instrument, with an emission current of 15 mA during

analysis. For UV-Vis/NIR absorbance measurements, a Jasco V-670 UV-Vis/NIR spectrophotometer was used. To measure *ex situ* absorbance spectra, a potential of −1.0 V vs. Ag/AgCl was applied to the grating surfaces for 30 s in a 0.1 M $LiClO_4$ in polycarbonate solution before removing the grating surfaces from solution for spectroscopic analysis. To measure *in situ* absorbance spectra, UV-Vis/NIR measurements were collected while a potential of −1.0 V vs. Ag/AgCl was applied to the grating surfaces in a 0.1 M $LiClO_4$ in polycarbonate solution.

Optical diffraction analysis. For diffraction and transmittance measurements, the grating surface was placed in an electrochemical cell connected to a potentiostat (Palmsens3, Palmsens) in a three-electrode setup. The grating sample was placed in a 0.1 M $LiClO_4$ in polycarbonate solution under alternating step potentials of −1.0 V and +1.0 V (15 s at each potential for a total duration of 250 s) vs. a Ag/AgCl reference electrode and in the presence of a Pt counter electrode. Light from a HeNe laser (λ = 633nm, 12 mW, LHRP-1201, Research Electro-Optics), *p*-polarized using a polarizer (Newport), was emitted and chopped at a frequency of 1.0 kHz using an optical chopper (Stanford Research Instruments SR540). A transmission geometry was employed in these optical measurements, where the intensities of the diffracted light (at the $n = 1$ spot) and transmitted light (at the $n = 0$ spot) were measured by a photodiode (Hamamatsu) connected to a DSP lock-in amplifier (EG&G model 7220). The photodiode potentials were recorded by a Labview program. For %T measurements at the $n = 0$ spot, a FTO glass substrate was used as reference. For %DE measurements, the photodiode intensities at the $n = 1$ spot were divided by the photodiode intensity at the $n = 0$ spot at +1.0 V vs. Ag/AgCl (when the grating is at its most transmissive state).

Results and Discussion

a) Electrodeposition and Characterization of ZnO-WO_3 and ZnO-PEDOT Gratings.

WO_3 electrodeposition. The mechanism of WO_3 electrodeposition from acidic peroxytungstatic acid ($H_2W_2O_{11}$) solutions has been described previously by other researchers.[40-41] Electrodeposition occurred at negative potentials (−0.4 V vs. Ag/AgCl for 150 s) through a combination of electrochemical reduction and disproportionation of the four peroxide (O_2^{2-}) anions in the peroxytungstate ions as described in Equation 1, where x is either 0, 4 or 8:

$$W_2O_{11}^{2-} + (2+x)\,H^+ + xe^- \rightarrow 2WO_3 + \frac{(2+x)}{2}H_2O + \frac{(8-x)}{4}\,O_2 \qquad (1)$$

If $x = 8$, then all four of the peroxide anions are reduced electrochemically to three O^{2-} ions (in the electrodeposited WO_3) and five H_2O. If $x = 0$, then the four peroxide anions disproportionate to form three O^{2-} ions, H_2O and two O_2. In addition to the peroxide reduction, a non-stoichiometric amount of W^{6+} ions in the WO_3 are also reduced to W^{5+}:

$$zH^+ + WO_3 + ze^- \rightarrow H_zWO_3 \qquad (2)$$

This tungsten reduction is verified by the observation of a blue color of the electrodeposited WO_3 film.

PEDOT electrodeposition. A PEDOT film was formed by the electrodeposition of 3,4-ethylenedioxythiophene (EDOT) using a slightly modified procedure of a previously reported method.[42-45] To generate stable, uniform PEDOT films, it was necessary to first spincoat a thin layer of PEDOT:PSS solution onto the FTO glass substrate to enhance conductivity and improve wetting of the surface, followed by the electropolymerization of EDOT to form a thicker layer of PEDOT. For the electrodeposition, an aqueous plating solution consisting of 0.02 M EDOT, 0.1 M SDS and 0.1 M $LiClO_4$ was employed. A constant potential of +1.0 V vs. Ag/AgCl was applied for 45 s to a photopatterned FTO glass substrate in the presence of a Pt counter electrode,

creating a large-scale (on the squared cm scale) uniform electroactive film. The electrodeposited film is in the reduced state, as evidenced by its blue color.

ZnO electrodeposition. Nanostructured ZnO was selectively deposited electrochemically on top of the WO_3 or PEDOT thin film. In our approach, 0.1 M aqueous zinc nitrate at pH 4.0 heated to 70°C was used as the plating solution, and electrodeposition occurred for 600 s at a potential of −0.9 V vs. Ag/AgCl to ensure full coverage of ZnO over WO_3 or PEDOT gratings. An SEM image of a ZnO-PEDOT grating sample with a ZnO electrodeposition time of 300 s, as shown in Supporting Information Figure S1, revealed sparse coverage of ZnO on the grating surface. The mechanism of the ZnO electrodeposition process has been discussed in previous works,[7, 46-47] and is summarized as follows: At a sufficiently negative applied potential, OH^- ions are generated, likely via the reduction of NO_3^- (eqn (4)). The OH^- and the Zn^{2+} ions then result in the precipitation of ZnO onto the working electrode of either WO_3 or PEDOT gratings (eqn (5)).

$$NO_3^- + H_2O + 2e^- \rightarrow NO_2^- + 2OH^- \quad (4)$$

$$Zn^{2+} + 2OH^- \rightarrow ZnO \downarrow + H_2O \quad (5)$$

Grating fabrication. The ZnO-WO_3 and ZnO-PEDOT gratings were fabricated using a combination of photolithography and electrodeposition. As shown in the scheme in Figure 1, after a layer of photoresist was spincoated onto conductive FTO glass slides, UV photopatterning was employed to create an array of photoresist stripes of width d_1 = 5 μm that were separated by 10 μm spacings of glass substrate. WO_3 or PEDOT was then selectively deposited electrochemically onto the exposed glass to form arrays of continuous micron-scale stripes of width d_2 = 10 μm. After the electrodeposition of both the electrochromic and ZnO layers, the photoresist was removed using acetone to create a diffraction grating surface that consists of an array of 10 μm wide ZnO-WO_3 or ZnO-PEDOT stripes separated by 5 μm wide spacings. The

morphology of the ZnO-WO_3 and ZnO-PEDOT diffraction gratings was characterized using a combination of SEM, AFM, and XPS. A cross-sectional SEM image in Figure 1f shows the various components of a sample composite ZnO-PEDOT grating, while SEM images in Figure 2 shows a) ZnO-WO_3 gratings and b) ZnO-PEDOT gratings that are composed of an array of 10 μm wide stripes that extend continuously over a length of several microns with 5 μm spacings in between. It should also be noted that the lower contrast in Figure 2b compared to 2a is due to the presence of a thin layer of PEDOT:PSS in the 5 μm spacings between the ZnO-PEDOT stripes in the ZnO-PEDOT gratings (since a thin layer of PEDOT:PSS was spincoated onto the FTO glass substrate to ensure stable electropolymerized PEDOT thin films), whereas the ZnO-WO_3 stripes are separated by 5 μm spacings of glass substrates in the ZnO-WO_3 gratings. The insets of the SEM images show high-resolution images of the nanostructured ZnO, where the individual flake-like ZnO nanostructures on the surface are depicted. This is a contrast to the mostly planar and featureless morphology of the WO_3 or PEDOT gratings before the addition of the ZnO layer, as confirmed by SEM images in Supporting Information Figure S2. In addition, AFM measurements (see Supporting Information Figure S3) reveal that an electrochromic layer of height h_1 = 200 nm was formed, and a nanostructured ZnO layer of height h_2 = 600 nm was formed. Furthermore, XPS measurements confirmed the formation of ZnO over both the WO_3 and PEDOT grating surfaces (Supporting Information Figure S4).

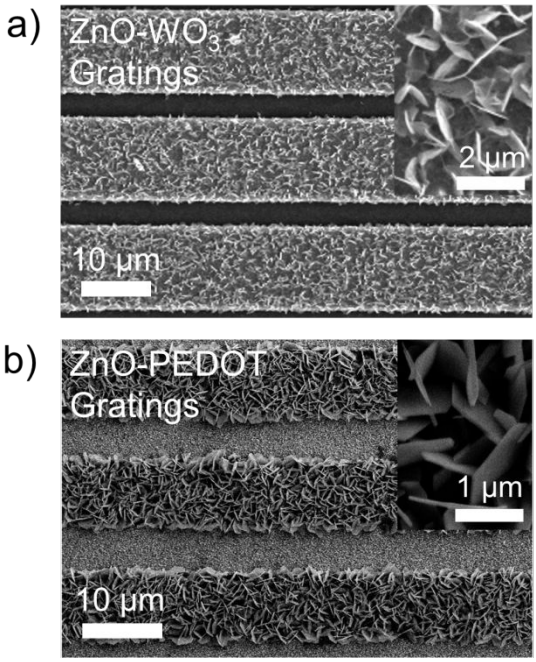

Figure 2. SEM images of a set of a) ZnO-WO_3 and b) ZnO-PEDOT gratings. The insets show high-resolution images of the nanostructured ZnO overlayer decorating the gratings.

b) Absorbance Spectra of ZnO-WO_3 and ZnO-PEDOT Gratings.

The absorbance spectra of the composite gratings were measured using a normal incidence transmission geometry, and it was revealed that the addition of a nanostructured ZnO overlayer on both the WO_3 and PEDOT gratings resulted in enhanced light absorption capabilities. The UV-Vis/NIR absorbance spectra for an electrodeposited WO_3 thin film (blue curve), an electrodeposited WO_3 grating (red curve) and an electrodeposited composite ZnO-WO_3 grating (black curve) are all shown in Figure 3a. These three *ex situ* spectra were obtained from samples that were first held at an applied potential of −1.0 V vs. Ag/AgCl for 30 s in an electrochemical cell containing a 0.1 M $LiClO_4$ solution, then removed for spectroscopic measurements. Absorbance measurements were presented *ex situ* since the spectral changes for our samples were greatest when measurements were performed in air. *In situ* measurements in

$LiClO_4$ solution were also taken to confirm that the absorbance spectra displayed similar visual qualities, as shown in Supporting Information Figure S5. As seen in Figure 3a, there is a strong absorbance peak around 1000 nm for the both the planar WO_3 thin films and the WO_3 gratings. Photographs of these two surfaces are also shown in Figure 3a and both exhibit the well-known blue color associated with reduced WO_3 electrochromic films. The spectrum of the WO_3 grating shows a slightly stronger absorption band than the planar thin film, and thus the color of the WO_3 grating is a darker blue.

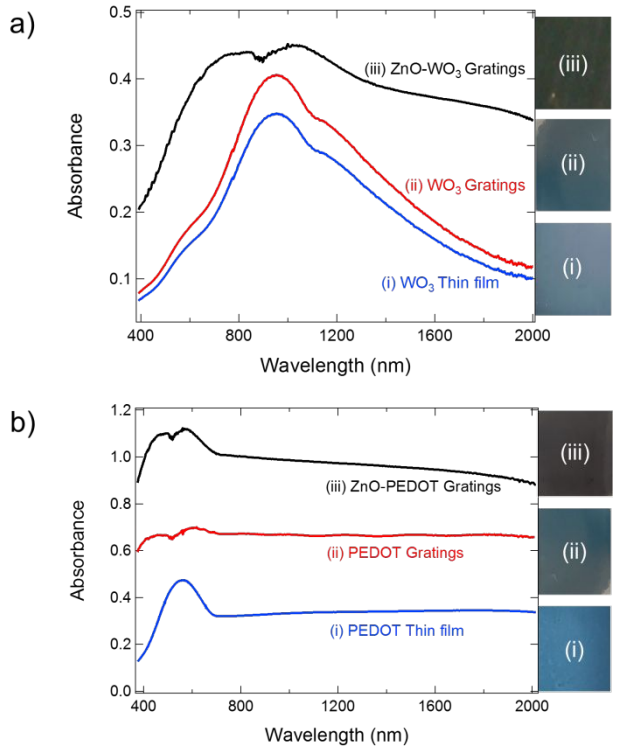

Figure 3. a) UV-Vis/NIR spectra of ZnO-WO_3 gratings, WO_3 gratings, and WO_3 thin film. b) UV-Vis/NIR spectra of ZnO-PEDOT gratings, PEDOT gratings, and PEDOT thin film. Photographs of each sample are also shown.

In contrast, the spectrum of the ZnO-WO_3 grating shows significantly enhanced absorbance at all wavelengths from 400 nm to 2000 nm. The addition of the nanostructured ZnO

overlayer must enhance the light absorption capabilities of the WO_3 grating underneath, since the electrodeposited ZnO has a high refractive index but no absorptive component ($\kappa = 0$). The UV-Vis/NIR absorbance spectrum of ZnO does not exhibit any absorption bands from 400 nm to 2000 nm, due to its high bandgap of 3.3 eV (375 nm).[48] Nevertheless, the addition of ZnO to form the ZnO-WO_3 gratings significantly enhances the optical absorption of the WO_3 gratings. The enhanced absorption also results in changes in visual appearance of the ZnO-WO_3 gratings, which becomes black as shown in Figure 3a. This data clearly shows that there is a significant amount of light coupled or redirected from the nanostructured ZnO overlayer to the underlying WO_3 portion of the grating structure.

A similar effect was observed for ZnO-PEDOT gratings. The UV-Vis/NIR absorbance spectra of an electrodeposited planar PEDOT thin film, an electrodeposited PEDOT grating, and an electrodeposited ZnO-PEDOT grating are shown in Figure 3b. It has been shown previously that PEDOT thin films exhibit a π to π^* transition with a bad gap of 1.7 eV (775 nm), thus PEDOT thin films in the reduced state show significant optical absorption near 600 nm,[31-32, 49] as evidenced by the blue trace in Figure 3b. Similar to the WO_3, PEDOT films also have a characteristic blue color in the reduced state as seen in the inset to Figure 3b. The PEDOT grating adds an additional absorption band at 450 nm (see Figure 3b) that has been attributed to an interference effect of the PEDOT grating, and is a darker blue in color as seen in the Figure 3b inset. As in the case of the ZnO-WO_3 gratings, the ZnO-PEDOT gratings also show a broadband enhancement in the UV-Vis/NIR absorbance spectrum, and has a black visual appearance, also seen in the inset of Figure 3b. We attribute this enhanced absorption from of ZnO-PEDOT gratings to the same mechanism as in the of ZnO-WO_3 gratings: coupling or redirection of light from the nanostructured ZnO overlayer to the underlying PEDOT grating.

c) Electrodiffraction of ZnO-WO_3 and ZnO-PEDOT Gratings. While the nanostructured ZnO overlayer enhances the absorptive properties of WO_3 and PEDOT gratings, there is an even larger effect on the electrochemically modulated diffraction. Electrodiffraction from electrodeposited ZnO-WO_3 and ZnO-PEDOT gratings at λ= 633 nm was measured *in situ* at normal incidence in an electrochemical cell containing 0.1 M $LiClO_4$ in polycarbonate, as shown schematically in Figure 4a. A representative diffraction pattern is shown in Figure 4b.

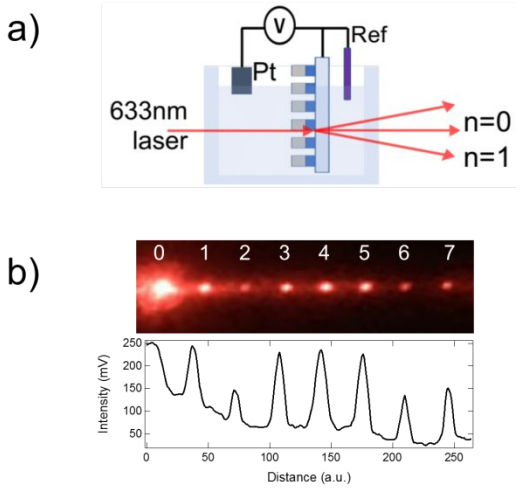

Figure 4. a) Schematic of the setup used for electrochemically modulated optical measurements of ZnO-WO_3 and ZnO-PEDOT gratings. b) Photograph of and intensity profile of diffraction pattern created by a set of ZnO-WO_3 gratings.

To measure the electrodiffractive and electrochromic response, the applied potential to a ZnO-WO_3 or ZnO-PEDOT grating was stepped between −1.0 V to +1.0 V vs. Ag/AgCl every 15 seconds. The current transients from the potential steps are shown in Figure 5. The current transients are higher for the ZnO-WO_3 grating as compared to the WO_3 grating, as shown in Figure 5b; we attribute this to the larger charging currents for high surface area nanostructured ZnO. Similar trends were observed for the ZnO-PEDOT and PEDOT gratings in Figure 5c.

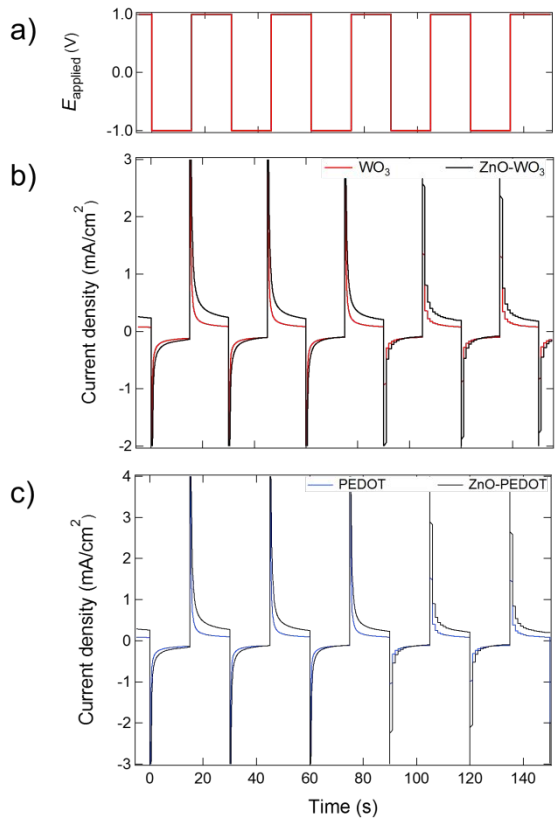

Figure 5. a) For the applied step potentials of −1.0 V and +1.0 V vs. Ag/AgCl, corresponding current transients for b) ZnO-WO_3 and WO_3 gratings, as well as c) ZnO-PEDOT and PEDOT gratings are shown.

The electrochemically modulated optical signals for electrochromic changes (transmission at $n = 0$) and first order diffraction ($n = 1$) were acquired as a function of time from both ZnO-WO_3 gratings (Figures 6b and 6c) and ZnO-PEDOT gratings (Figures 7b and 7c). Transmission measurements at $n = 0$ were collected *in situ* at normal incidence at $\lambda = 633$ nm in an electrochemical cell containing 0.1 M $LiClO_4$ in polycarbonate using a FTO coated glass slide as reference. To ensure reproducibility, optical measurements were acquired as the applied potentials were stepped between +1.0 V and –1.0 V (potentials measured against Ag/AgCl) for a total of 10 times. The %T observed in Figure 6b from the $n = 0$ spot for both WO_3 gratings and

ZnO-WO_3 gratings varied reversibly with the applied potential as a result of the electrochromic properties of WO_3. For the WO_3 grating, %T switched between 79% at +1.0 V to 27% at −1.0 V vs. Ag/AgCl. This variation in %T is indicative of the electrochromic effects displayed by the WO_3 grating, with larger Δ%T values indicating a greater optical contrast under an applied potential. At −1.0 V, Li ion intercalation and electron injection into the WO_3 grating lead to an increase in κ and thus the large increase (Δ%T = 52%) in light absorption. This effect has been observed previously, on both planar WO_3 films and gratings.[24-26] Similar electrochromic effects were observed for the ZnO-WO_3 gratings, with a Δ%T = 46%. However, the average intensity of the transmitted light was lower for the ZnO-WO_3 gratings as compared to undecorated WO_3 gratings (T_{ave} = 40% vs T_{ave} = 55%). This decrease is expected from the absorption spectra results discussed in the previous section.

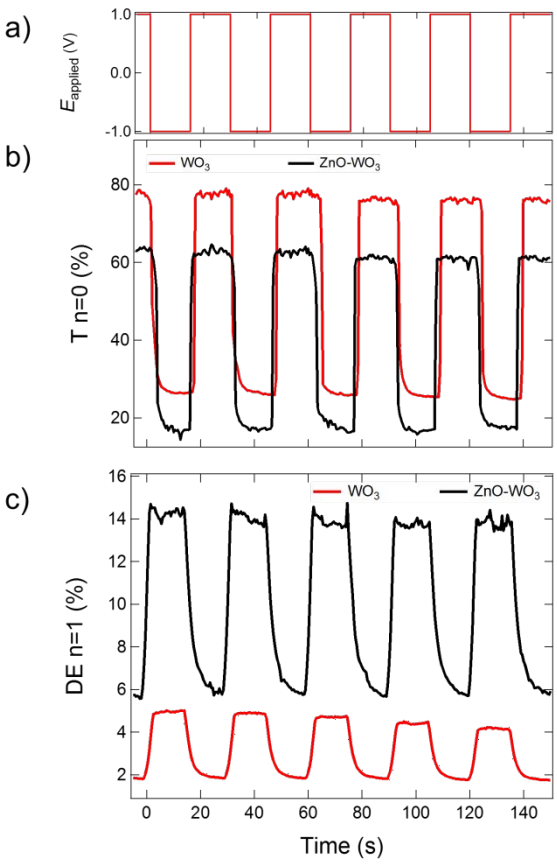

Figure 6. Optical measurements of ZnO-WO_3 and WO_3 gratings after a) applied potentials of −1.0 V and +1.0 V vs. Ag/AgCl showing the b) transmittance at the n = 0 spot and the c) diffraction efficiency at the n = 1 spot.

Then, for electrodiffraction experiments, optical measurements were also collected *in situ* at normal incidence at λ = 633 nm in an electrochemical cell containing 0.1 M $LiClO_4$ in polycarbonate using the gratings' n = 0 transmission measurements at +1.0 V vs. Ag/AgCl (the gratings' most transmissive state) as reference. To ensure reproducibility, %DE measurements were reported as the applied potentials were stepped between +1.0 V and –1.0 V (potentials measured against Ag/AgCl) for a total of 10 times. In contrast to the electrochromic behavior, both the average and the electrochemically modulated diffraction efficiency (%DE) observed for

the n =1 diffraction spot were greater for the ZnO-WO_3 gratings compared to the WO_3 gratings. It should also be noted that the electrochemical modulation of %DE was 180° out of phase with the modulation of %T. A comparison of Figures 6b and 6c revealed that the more absorptive state at n = 0 (for the applied potential −1.0 V vs. Ag/AgCl) displayed a low %T but a high %DE, and vice versa at +1.0 V vs. Ag/AgCl. From the red trace in Figure 6c, an average %DE of 3.2% and an electrochemically modulated Δ%DE of 2.4% were observed for WO_3 gratings. As for the ZnO-WO_3 gratings (black trace in Figure 6c), the average %DE increased to 10%, and the electrodiffraction increased to a Δ%DE of 9.7% – four times higher than the gratings without ZnO. A similar effect was observed for the case of the ZnO-PEDOT and PEDOT gratings. As seen in the Figure 7b, for PEDOT gratings, %T and Δ%T were 45% and 35% respectively; these values decreased to 36% and 27% for ZnO-PEDOT gratings. However, the diffraction efficiencies again showed significant increases: an average %DE and Δ%DE were 3.5% and 2.8% for PEDOT gratings, but increased significantly to 8.5% and 8.3% respectively as shown in Figure 6c. The drastic increase of Δ%DE displayed by the ZnO-WO_3 and ZnO-PEDOT gratings compared to their counterpart WO_3 and PEDOT gratings indicates a significant improvement of their electrodiffractive performance, likely due to optical coupling between ZnO and the host material. By reporting Δ%DE values, we have demonstrated that we are able to quantify optical coupling between the non-absorptive nanostructured ZnO overlayer and the absorptive host material (WO_3 and PEDOT).

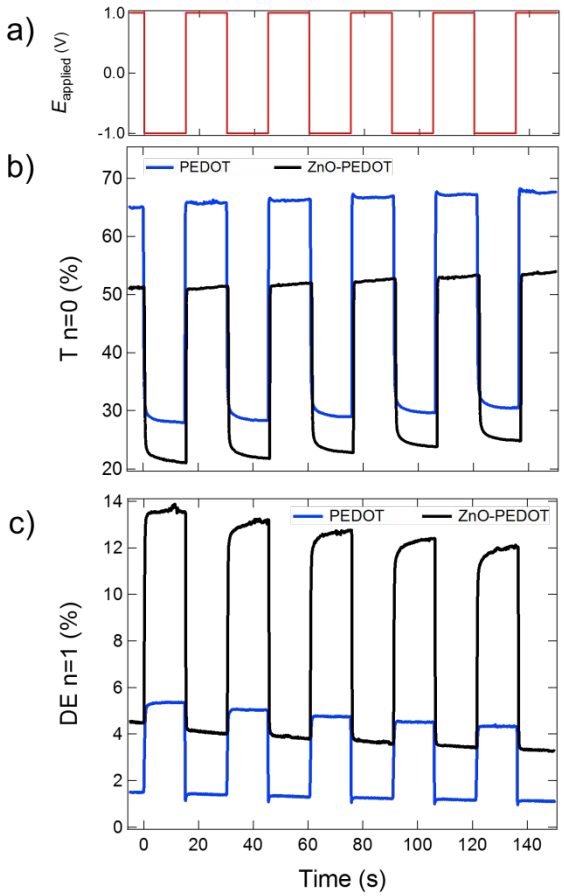

Figure 7. Optical measurements of ZnO-PEDOT and PEDOT gratings after a) applied potentials of −1.0 V and +1.0 V vs. Ag/AgCl showing the b) transmittance at the n = 0 spot and the c) diffraction efficiency at the n = 1 spot.

To understand these changes in the average %DE and Δ%DE, we need to consider the contributions to η and κ for the composite gratings. In the case of thin gratings, the diffraction efficiency *DE* is a linear combination of an absorptive component and a phase component (eqn (6)):[22, 38, 50]

$$DE = a(\Delta\kappa)^2 + b(\Delta\eta)^2 \qquad (6)$$

This equation can be used to explain the increases in the average %DE, but not the electrodiffractive component (Δ%DE). For the case of the composite ZnO-WO_3 and ZnO-

PEDOT gratings in this paper, an additional coupling between the ZnO and the absorptive WO_3 or PEDOT is observed, even though no electrodiffractive effect ($\Delta\kappa = \Delta\eta = 0$) is observed with ZnO gratings alone (optical measurements shown in Supporting Information Figure S6). Instead, the nanostructured ZnO overlayer redirects light into the electrochromic WO_3 or PEDOT component of the grating. This type of optical coupling occurs because the electrodeposited nanostructured ZnO coating is on the same scale as the light; similar optical effects have been previously observed in calculations of the diffraction efficiency of taller gratings.[35, 50] Furthermore, the high surface area, nanostructured nature of the ZnO provides an additional coupling mechanism via a series of total internal reflection from the ZnO to the absorptive material underneath.[6] To support our proposed mechanism for optical coupling, we showed that ZnO-PEDOT gratings without a fully covered ZnO overlayer displayed much weaker electrodiffractive effects (see Supporting Information Figure S7). ZnO-PEDOT gratings with a sparse ZnO overlayer only displayed a 1.5-fold enhancement of Δ%DE compared to PEDOT gratings, which indicates weaker optical coupling between the sparse ZnO overlayer and the absorptive material underneath. Thus, the presence of the electrodeposited ZnO, in a combination of the nanoscale structure and metamaterial patterning, is crucial for creating enhanced electrodiffraction.

Conclusions

The enhanced absorption and electrodiffraction observed from the composite ZnO-WO_3 and ZnO-PEDOT gratings described in this paper clearly demonstrate that there is a strong optical coupling between the electrodeposited nanostructured ZnO overlayer and the electrochromic thin film layer underneath. This coupling has some significant implications; the presence of both nanoscale structuring and metamaterial patterning (e.g., gratings, nanocone

arrays, or nanoring arrays) are both required for this coupling to occur. The electrodiffraction from these gratings increases in the presence of the high surface area nanostructured ZnO, even though the ZnO itself has no absorptive (κ) or electrochromic ($\Delta\kappa$) behavior. In these gratings, the ZnO enhances the delivery of light to the underlying electrochromic materials via optical coupling. We have also observed this coupling effect previously in the enhanced antireflectivity of PEDOT and gold nanocone arrays that were coated with electrodeposited ZnO nanostructures.[7] Going forward, we should be able to employ this coupling effect to enhance the production of electron-hole pairs by enhancing the optical absorption of TiO_2, In_2O_3, or Si semiconductor patterned gratings, nanocone arrays, or nanoring arrays.

Supporting Information

The following are available free of charge: (i) SEM images of sparsely ZnO covered ZnO-PEDOT gratings after applying a ZnO electrodeposition time of 300 s, (ii) SEM images of WO_3 and PEDOT gratings, (iii) AFM measurements of ZnO coated gratings, (iv) XPS of ZnO coated gratings, (v) absorbance spectra of ZnO-PEDOT and PEDOT gratings performed *in situ*, (vi) optical measurements for the transmission and diffraction efficiency of ZnO only gratings, and (vii) optical measurements for the transmission and diffraction efficiency of ZnO-PEDOT gratings with a sparse ZnO overlayer.

Notes

The authors declare no competing financial interests.

Acknowledgments

This work was supported by the National Science Foundation through grant CHE-1403506. SEM and XPS analyses were performed at the Irvine Materials Research Institute (IMRI) at UC Irvine. UV-Vis/NIR measurements were performed at the UC Irvine Laser Spectroscopy Labs. The authors would also like to thank the Penner Group for their help with AFM measurements.

References

1. Murakoshi, K.; Yanagida, S.; Capel, M.; Castner, E. W. Interfacial Electron Transfer Dynamics of Photosensitized Zinc Oxide Nanoclusters. In *Nanostructured Materials*, American Chemical Society: 1997; Vol. 679, pp 221-238.

2. Conradt, J.; Sartor, J.; Thiele, C.; Maier-Flaig, F.; Fallert, J.; Kalt, H.; Schneider, R.; Fotouhi, M.; Pfundstein, P.; Zibat, V.; Gerthsen, D. Catalyst-Free Growth of Zinc Oxide Nanorod Arrays on Sputtered Aluminum-Doped Zinc Oxide for Photovoltaic Applications. *J. Phys. Chem. C* **2011,** *115*, 3539-3543.

3. Gonzalez-Valls, I.; Lira-Cantu, M. Vertically-Aligned Nanostructures of ZnO for Excitonic Solar Cells: A Review. *Energy Environ. Sci.* **2009,** *2*, 19-34.

4. Müller, J.; Rech, B.; Springer, J.; Vanecek, M. TCO and Light Trapping in Silicon Thin Film Solar Cells. *Sol. Energy* **2004,** *77*, 917-930.

5. Battaglia, C.; Escarré, J.; Söderström, K.; Charrière, M.; Despeisse, M.; Haug, F.-J.; Ballif, C. Nanomoulding of Transparent Zinc Oxide Electrodes for Efficient Light Trapping in Solar Cells. *Nat. Photon.* **2011,** *5*, 535.

6. Lin, A.; Phillips, J. Optimization of Random Diffraction Gratings in Thin-Film Solar Cells using Genetic Algorithms. *Sol. Energy Mater Sol. Cells* **2008,** *92*, 1689-1696.

7. Fung, H. W. M.; So, S.; Kartub, K.; Loget, G.; Corn, R. M. Ultra-Antireflective Electrodeposited Plasmonic and PEDOT Nanocone Array Surfaces. *J. Phys. Chem. C* **2017,** *121*, 22377-22383.

8. Yaqoob, Z.; Riza, N. A. Passive Optics No-Moving-Parts Barcode Scanners. *IEEE Photonics Technology Letters* **2004,** *16*, 954-956.

9. Boudoux, C.; Yun, S. H.; Oh, W. Y.; White, W. M.; Iftimia, N. V.; Shishkov, M.; Bouma, B. E.; Tearney, G. J. Rapid Wavelength-Swept Spectrally Encoded Confocal Microscopy. *Opt. Express* **2005,** *13*, 8214-8221.

10. Chen, J.; Bos, P. J.; Vithana, H.; Johnson, D. L. An Electro-Optically Controlled Liquid Crystal Diffraction Grating. *Appl. Phys. Lett.* **1995,** *67*, 2588-2590.

11. Glesk, I.; Bock, P. J.; Cheben, P.; Schmid, J. H.; Lapointe, J.; Janz, S. All-Optical Switching using Nonlinear Subwavelength Mach-Zehnder on Silicon. *Opt. Express* **2011,** *19*, 14031-14039.

12. Williams, G. V. M.; Do, M. T. T.; Raymond, S. G.; Bhuiyan, M. D. H.; Kay, A. J. Optically Switchable Diffraction Grating in a Photochromic/Polymer Thin Film. *Appl. Opt.* **2015,** *54*, 6882-6886.

13. P. Bousquet. *Spectroscopy and Its Instrumentation*; Hilger: London, 1971.

14. C. Palmer. *Diffraction Grating Handbook*, 6th ed.; Newport Corporation: New York, 2005.

15. Arafat Hossain, M.; Canning, J.; Ast, S.; Cook, K.; Rutledge, P. J.; Jamalipour, A. Combined "Dual" Absorption and Fluorescence Smartphone Spectrometers. *Opt. Lett.* **2015,** *40*, 1737-1740.

16. Yang, M.; Wang, H.; Li, M.; He, J.-J. In *An Echelle Diffraction Grating for Imaging Spectrometer*, SPIE Optical Engineering + Applications, SPIE: 2016; p 7.

17. Cheben, P.; Bock, P. J.; Schmid, J. H.; Lapointe, J.; Janz, S.; Xu, D.-X.; Densmore, A.; Delâge, A.; Lamontagne, B.; Hall, T. J. Refractive Index Engineering with Subwavelength Gratings for Efficient Microphotonic Couplers and Planar Waveguide Multiplexers. *Opt. Lett.* **2010,** *35*, 2526-2528.

18. Knop, K. Rigorous Diffraction Theory for Transmission Phase Gratings with Deep Reectangular Grooves. *J. Opt. Soc. Am.* **1978,** *69*, 1206-1210.

19. Botten, I. C.; Craig, M. S.; McPhedran, R. C.; Adams, J. L.; Andrewartha, J. R. The Dielectric Lamellar Diffraction Grating. *Optica Acta* **1981,** *28*, 413-428.

20. Kondrachova, L. V.; May, R. A.; Cone, C. W.; Vanden Bout, D. A.; Stevenson, K. J. Evaluation of Lithium Ion Insertion Reactivity via Electrochromic Diffraction-Based Imaging. *Langmuir* **2009,** *25*, 2508-2518.

21. Bailey, R. C.; Hupp, J. T. Large-Scale Resonance Amplification of Optical Sensing of Volatile Compounds with Chemoresponsive Visible-Region Diffraction Gratings. *JACS* **2002,** *124*, 6767-6774.

22. Schanze, K. S.; Bergstedt, T. S.; Hauser, B. T.; Cavalaheiro, C. S. P. Photolithographically-Patterned Electroactive Films and Electrochemically Modulated Diffraction Gratings. *Langmuir* **2000,** *16*, 795-810.

23. Massari, A. M.; Stevenson, K. J.; Hupp, J. T. Development and Application of Patterned Conducting Polymer Thin Films as Chemoresponsive and Electrochemically Responsive Optical Diffraction Gratings. *J. Electroanal. Chem.* **2001,** *500*, 185-191.

24. Mortimer, R. J.; Rosseinsky, D. R.; Monk, P. M. S. Electrochromic Materials and Devices, 1st ed.; Wiley-VCH Verlag GmbH & Co. KGaA: Berlin, 2015.

25. Mortimer, R. J. Electrochromic Materials. *Annu. Rev. Mater. Res.* **2011,** *41*, 241-268.

26. Somani, P. R.; Radhakrishnan, S. Electrochromic Materials and Devices: Present and Future. *Mater. Chem. Phys.* **2003,** *77*, 117-133.27.

27. Granqvist, C. G. Electrochromics for Smart Windows: Oxide-Based Thin Films and Devices. *Thin Solid Films* **2014,** *564*, 1-38.

28. Kirchmeyer, S.; Elschner, A.; Reuter, K.; Lovenich, W.; Merker, U. *PEDOT: Principles and Applications of an Intrinsically Conductive Polymer*; Eds.; CRC Press, 2010.

29. Sankaran, B.; Reynolds, J. R. High-Contrast Electrochromic Polymers from Alkyl-Derivatized Poly(3,4-ethylenedioxythiophenes). *Macromolecules* **1997,** *30*, 2582-2588.

30. Mortimer, R. J. Organic Electrochromic Materials. *Electrochim. Acta* **1999,** *44*, 2971-2981.

31. Kumar, A.; Welsh, D. M.; Morvant, M. C.; Piroux, F.; Abboud, K. A.; Reynolds, J. R. Conducting Poly(3,4-alkylenedioxythiophene) Derivatives as Fast Electrochromics with High-Contrast Ratios. *Chem. Mater.* **1998,** *10*, 896-902.

32. Ruffo, R.; Celik-Cochet, A.; Posset, U.; Mari, C. M.; Schottner, G. Mechanistic Study of the Redox Process of an *In Situ* Oxidatively Polymerised Poly(3,4-ethylene-dioxythiophene) Film. *Sol. Energy Mater. Sol. Cells* **2008,** *92*, 140-145.

33. Von Rottkay, K.; Rubin, M.; Wen, S. J. Optical Indices of Electrochromic Tungsten Oxide. *Thin Solid Films* **1997,** *306*, 10-16.

34. Pettersson, L. A. A.; Ghosh, S.; Inganäs, O. Optical Anisotropy in Thin Films of Poly(3,4-ethylenedioxythiophene)–Poly(4-styrenesulfonate). *Org. Electron.* **2002,** *3*, 143-148.

35. Dang, X.; Massari, A. M.; Hupp, J. T. Electrochemically Modulated Diffraction - A Novel Strategy for the Determination of Conduction-Band-Edge Energies for Nanocrystalline Thin-Film Semiconductor Electrodes. *Electrochem. Solid-State Lett.* **2000,** *3*, 555-558.

36. Kim, Y.; Kim, Y.; Kim, S.; Kim, E. Electrochromic Diffraction from Nanopatterned Poly(3-hexylthiophene). *ACS Nano* **2010,** *4*, 5277-5284.

37. Park, C.; Na, J.; Han, M.; Kim, E. Transparent Electrochemical Gratings from a Patterned Bistable Silver Mirror. *ACS Nano* **2017,** *11*, 6977-6984.

38. Tian, S.; Armstrong, N. R.; Knoll, W. Electrochemically Tunable Surface-Plasmon-Enhanced Diffraction Gratings and their (Bio-)sensing Applications. *Langmuir* **2005,** *21*, 4656-4660.

39. Matsui, T.; Ozaki, M.; Yoshino, K. In *Electro-Tunable Liquid Crystal Waveguide Laser*, Optical Science and Technology, the SPIE 49th Annual Meeting, SPIE: 2004; p 12.

40. Meulenkamp, E. A. Mechanism of WO_3 Electrodeposition from Peroxy-Tungstate Solution. *J. Electrochem. Soc.* **1997,** *144*, 1664-1671.

41. Cai, G.; Cui, M.; Kumar, V.; Darmawan, P.; Wang, J.; Wang, X.; Lee-Sie Eh, A.; Qian, K.; Lee, P. S. Ultra-Large Optical Modulation of Electrochromic Porous WO_3 Film and the Local Monitoring of Redox Activity. *Chem Sci.* **2016,** *7*, 1373-1382.

42. So, S.; Fung, H. W. M.; Kartub, K.; Maley, A. M.; Corn, R. M. Fabrication of PEDOT Nanocone Arrays with Electrochemically Modulated Broadband Antireflective Properties. *J. Phys. Chem. Lett.* **2017,** *8*, 576-579.

43. Randriamahazaka, H.; Sini, G.; Tran Van, F. Electrodeposition Mechanisms and Electrochemical Behavior of Poly(3,4-ethylenedithiathiophene). *J. Phys. Chem. C* **2007,** *111*, 4553-4560.

44. Nguyen, V.-Q.; Schaming, D.; Martin, P.; Lacroix, J.-C. Highly Resolved Nanostructured PEDOT on Large Areas by Nanosphere Lithography and Electrodeposition. *ACS Appl. Mater. Interfaces* **2015,** *7*, 21673-21681.

45. Donavan, K. C.; Arter, J. A.; Pilolli, R.; Cioffi, N.; Weiss, G. A.; Penner, R. M. Virus−Poly(3,4-ethylenedioxythiophene) Composite Films for Impedance-Based Biosensing. *Anal. Chem.* **2011,** *83*, 2420-2424.

46. Illy, B. N.; Cruickshank, A. C.; Schumann, S.; Da Campo, R.; Jones, T. S.; Heutz, S.; McLachlan, M. A.; McComb, D. W.; Riley, D. J.; Ryan, M. P. Electrodeposition of ZnO Layers for Photovoltaic Applications: Controlling Film Thickness and Orientation. *J. Mater. Chem.* **2011,** *21*, 12949-12957.

47. Sun, S.; Jiao, S.; Zhang, K.; Wang, D.; Gao, S.; Li, H.; Wang, J.; Yu, Q.; Guo, F.; Zhao, L. Nucleation Effect and Growth Mechanism of ZnO Nanostructures by Electrodeposition from Aqueous Zinc Nitrate Baths. *J. Cryst. Growth* **2012,** *359*, 15-19.

48. Xu, L.; Chen, Q.; Xu, D. Hierarchical ZnO Nanostructures Obtained by Electrodeposition. *J. Phys. Chem. C* **2007,** *111*, 11560-11565.

49. Deutschmann, T.; Oesterschulze, E. Micro-Structured Electrochromic Device Based on Poly(3,4-ethylenedioxythiophene). *J. Micromech. Microeng.* **2013,** *23*, 065032.

50. Nelson, K. A.; Casalegno, R.; Miller, R. J. D.; Fayer, M. D. Laser-Induced Excited State and Ultrasonic Wave Gratings: Amplitude and Phase Grating Contributions to Diffraction. *J. Chem. Phys.* **1982,** *77*, 1144-1152.

TOC Graphic

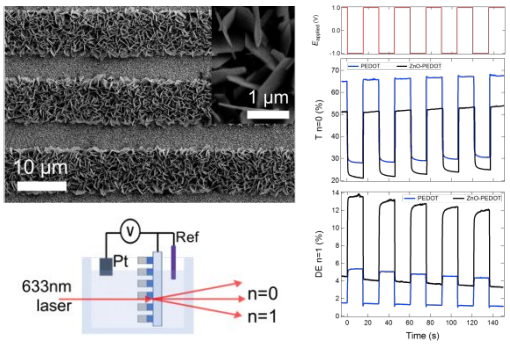

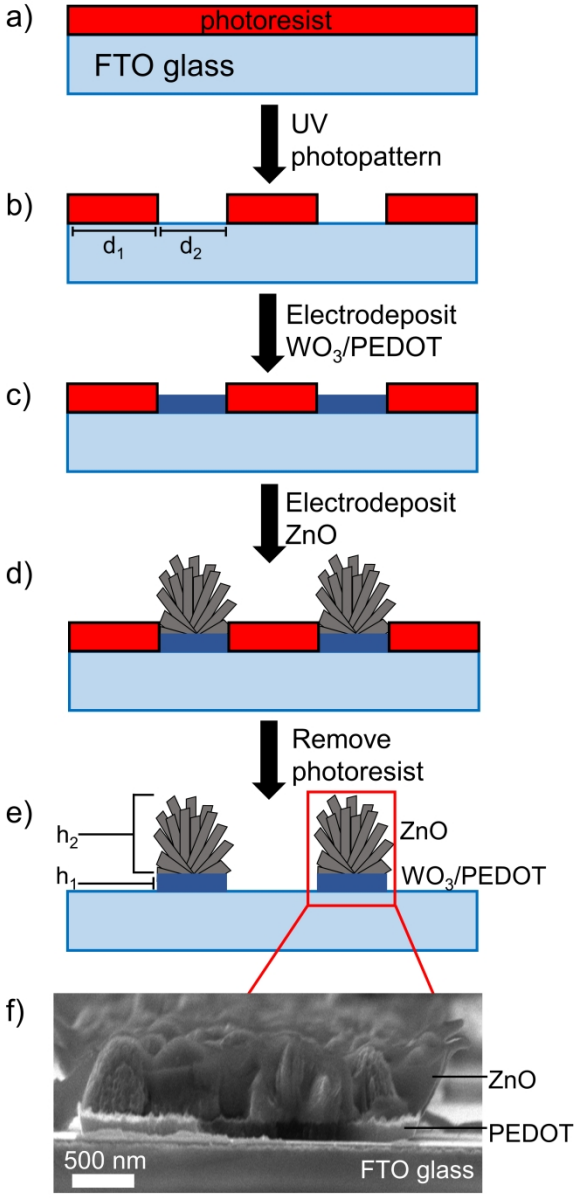

Figure 1. Schematic of the fabrication process of ZnO-WO_3 and ZnO-PEDOT gratings shown in a) – e). A cross-sectional SEM image f) reveals the various components of a sample ZnO-PEDOT grating.

216x440mm (300 x 300 DPI)

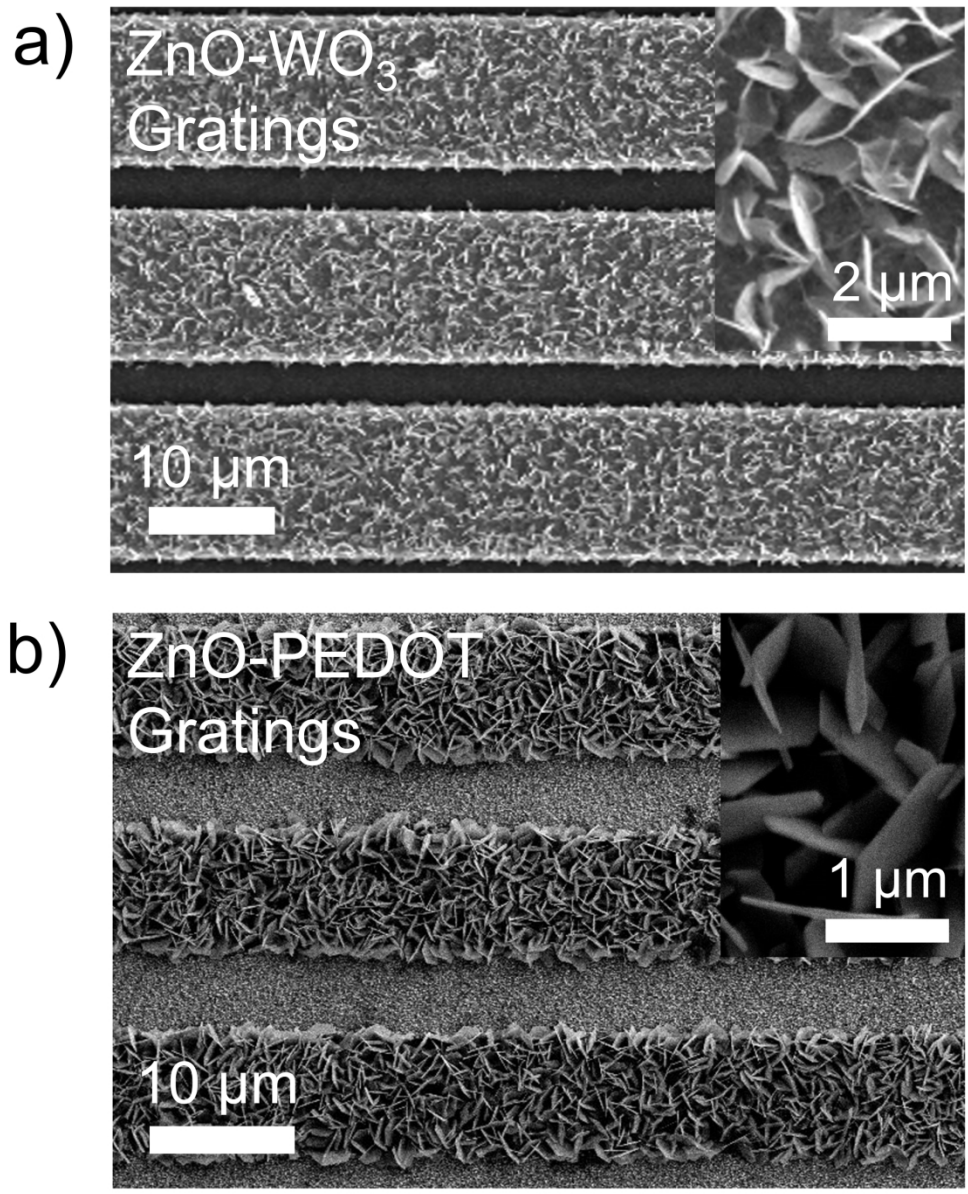

Figure 2. SEM images of a set of a) ZnO-WO_3 and b) ZnO-PEDOT gratings. The insets show high-resolution images of the nanostructured ZnO overlayer decorating the gratings.

216x268mm (300 x 300 DPI)

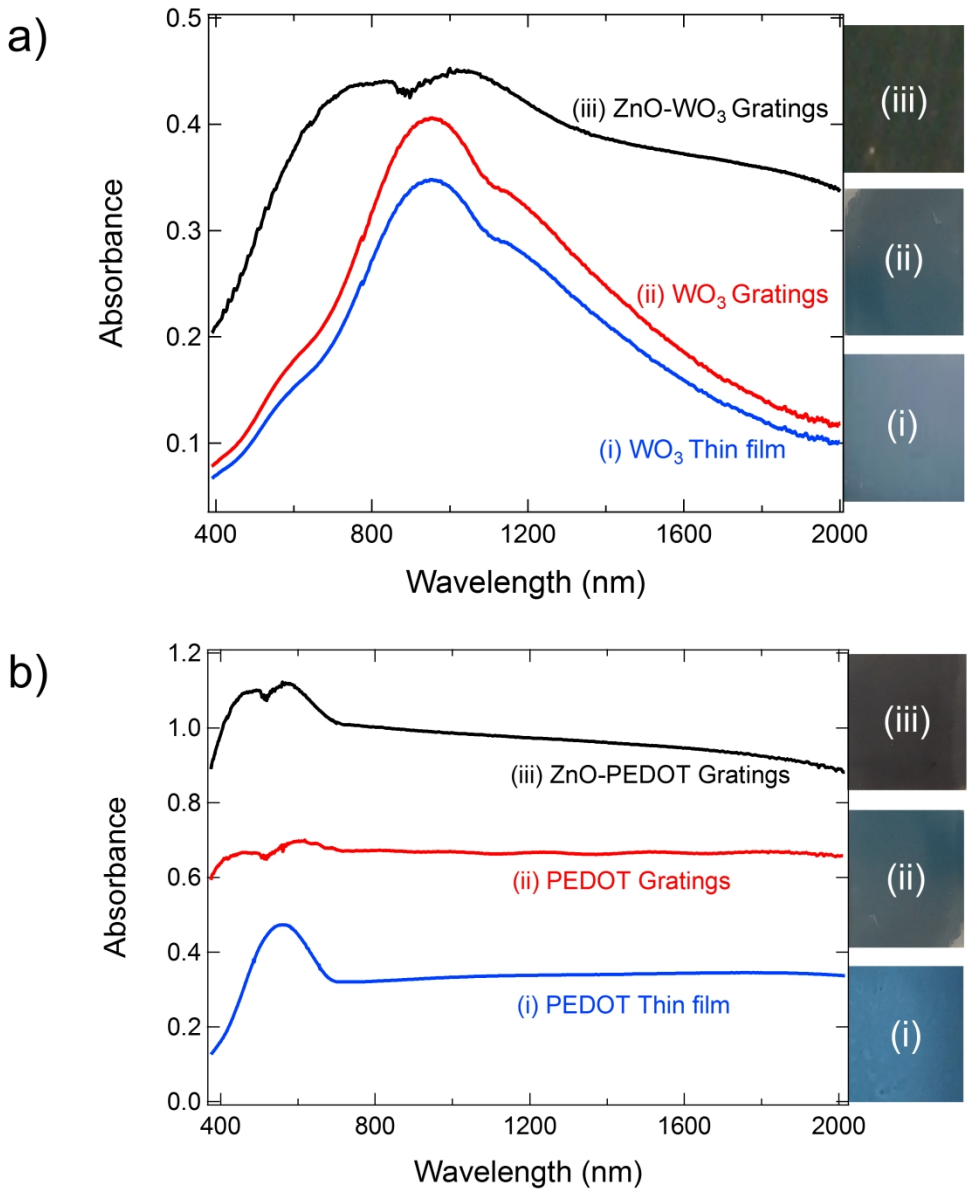

Figure 3. a) UV-Vis/NIR spectra of ZnO-WO_3 gratings, WO_3 gratings, and WO_3 thin film. b) UV-Vis/NIR spectra of ZnO-PEDOT gratings, PEDOT gratings, and PEDOT thin film. Photographs of each sample are also shown.

267x330mm (300 x 300 DPI)

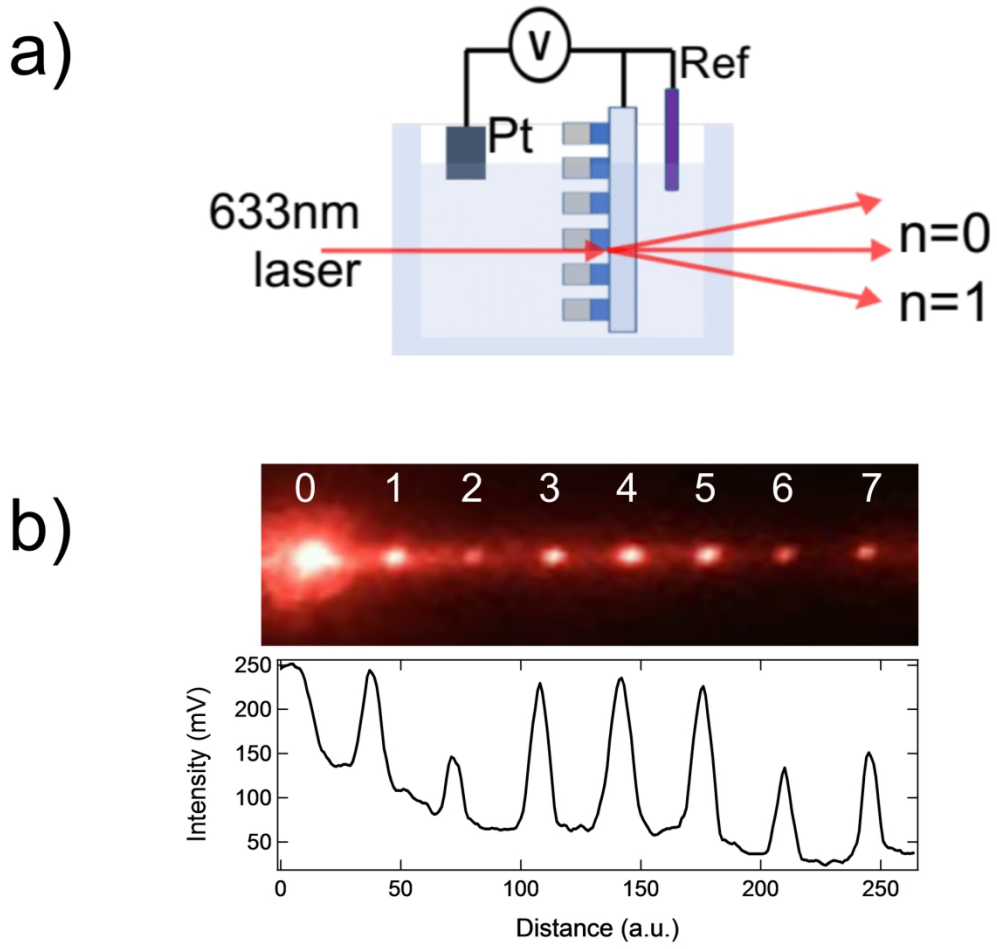

Figure 4. a) Schematic of the setup used for electrochemically modulated optical measurements of ZnO-WO_3 and ZnO-PEDOT gratings. b) Photograph of and intensity profile of diffraction pattern created by a set of ZnO-WO_3 gratings.

165x155mm (300 x 300 DPI)

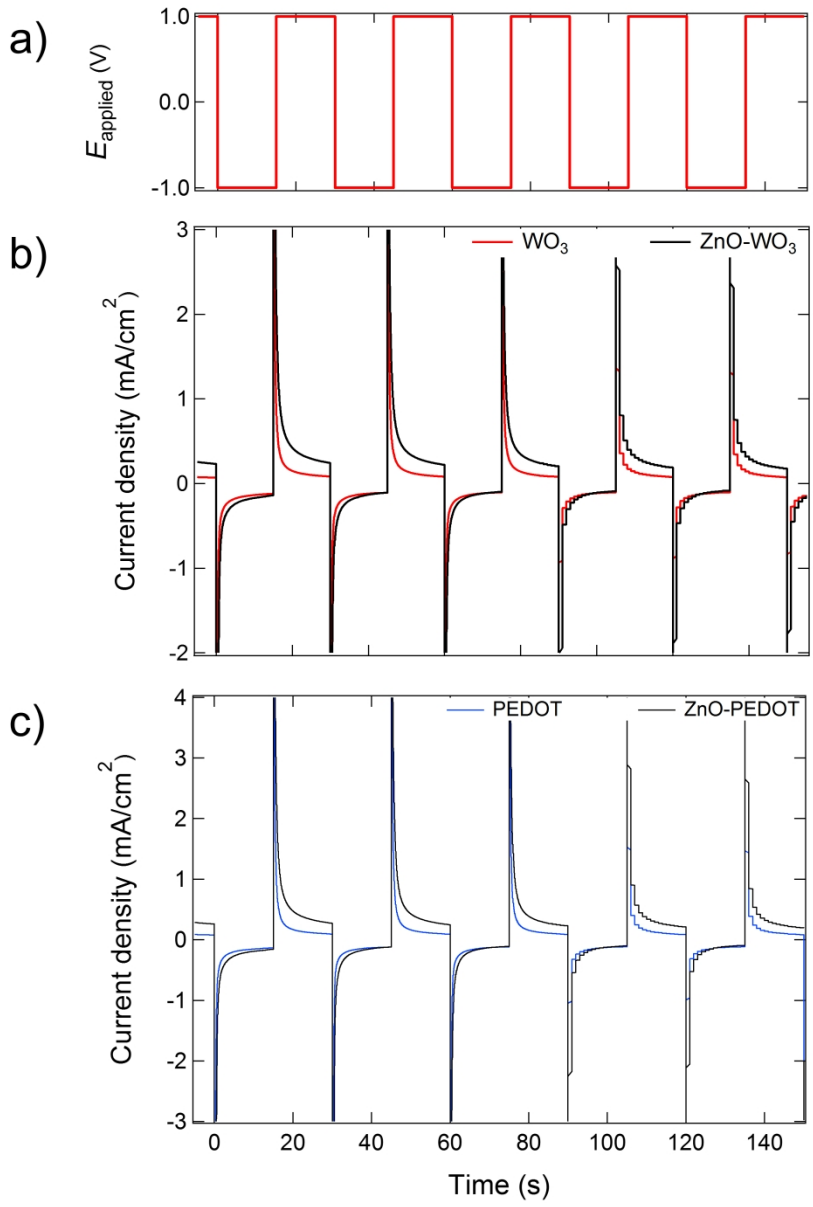

Figure 5. a) For the applied step potentials of −1.0 V and +1.0 V vs. Ag/AgCl, corresponding current transients for b) ZnO-WO_3 and WO_3 gratings, as well as c) ZnO-PEDOT and PEDOT gratings are shown.

236x347mm (300 x 300 DPI)

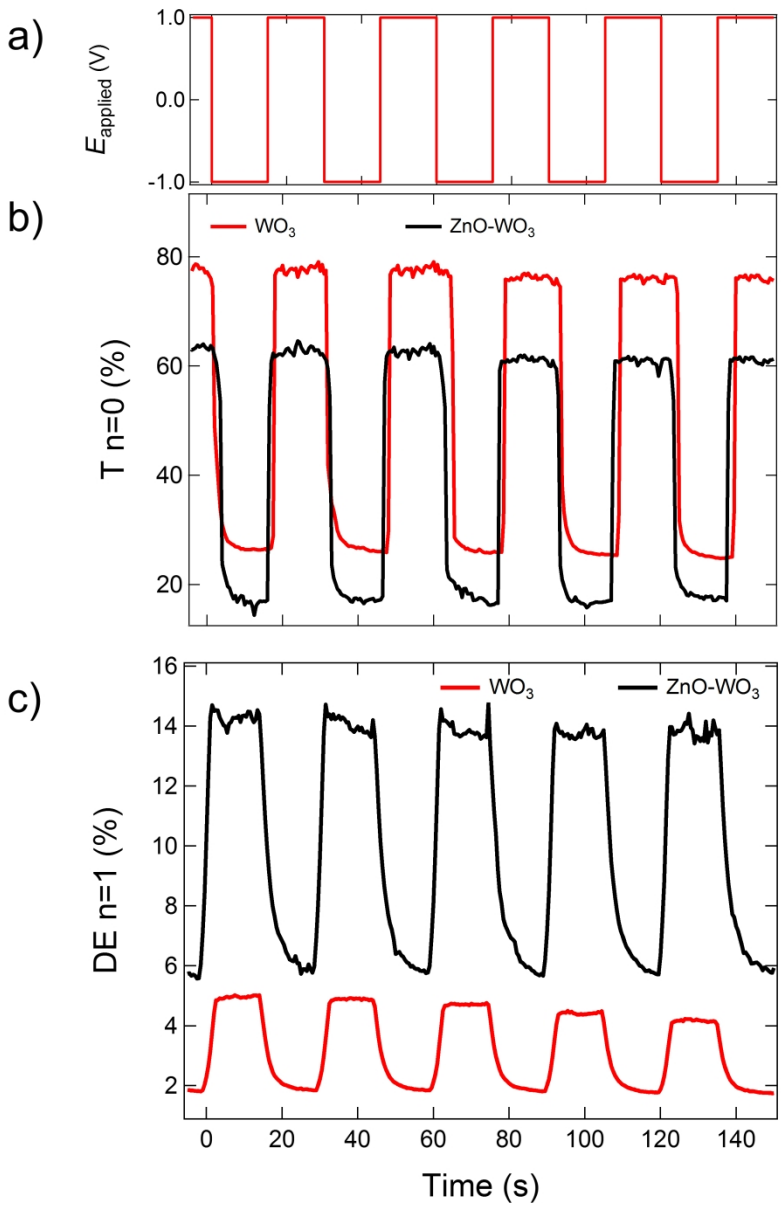

Figure 6. Optical measurements of ZnO-WO_3 and WO_3 gratings after a) applied potentials of −1.0 V and +1.0 V vs. Ag/AgCl showing the b) transmittance at the n = 0 spot and the c) diffraction efficiency at the n = 1 spot.

243x368mm (300 x 300 DPI)

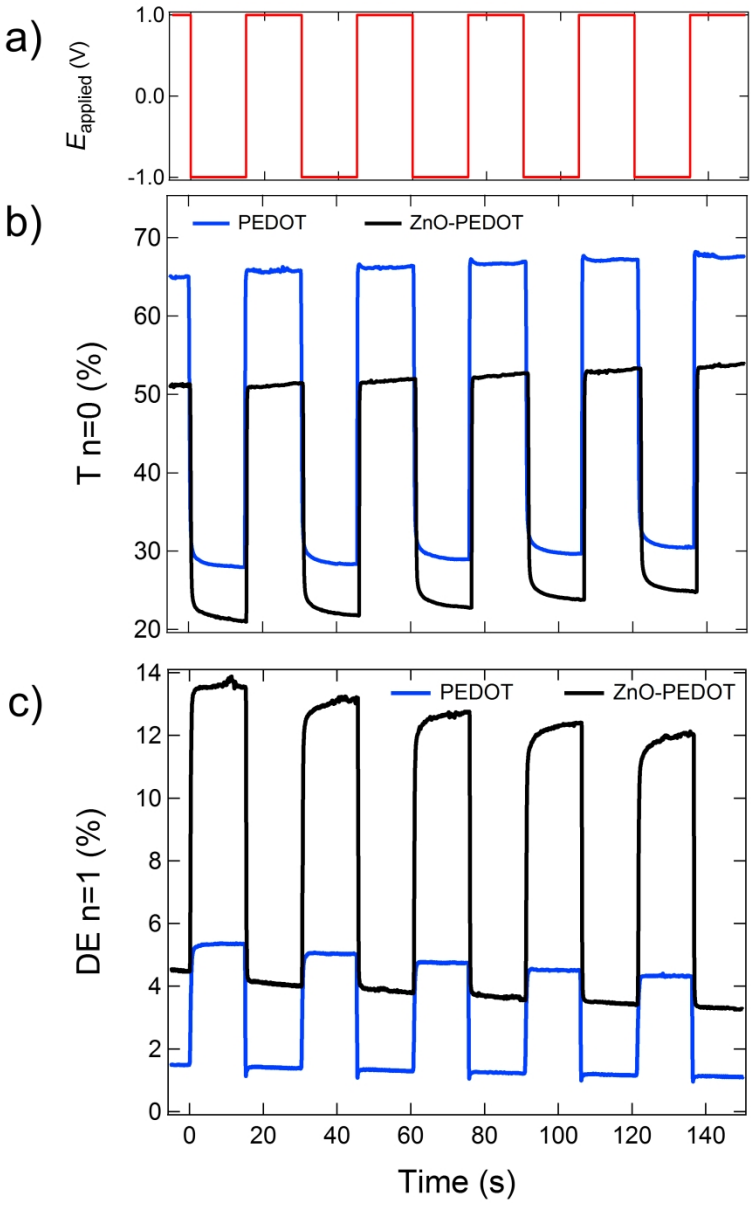

Figure 7. Optical measurements of ZnO-PEDOT and PEDOT gratings after a) applied potentials of −1.0 V and +1.0 V vs. Ag/AgCl showing the b) transmittance at the n = 0 spot and the c) diffraction efficiency at the n = 1 spot.

228x355mm (300 x 300 DPI)

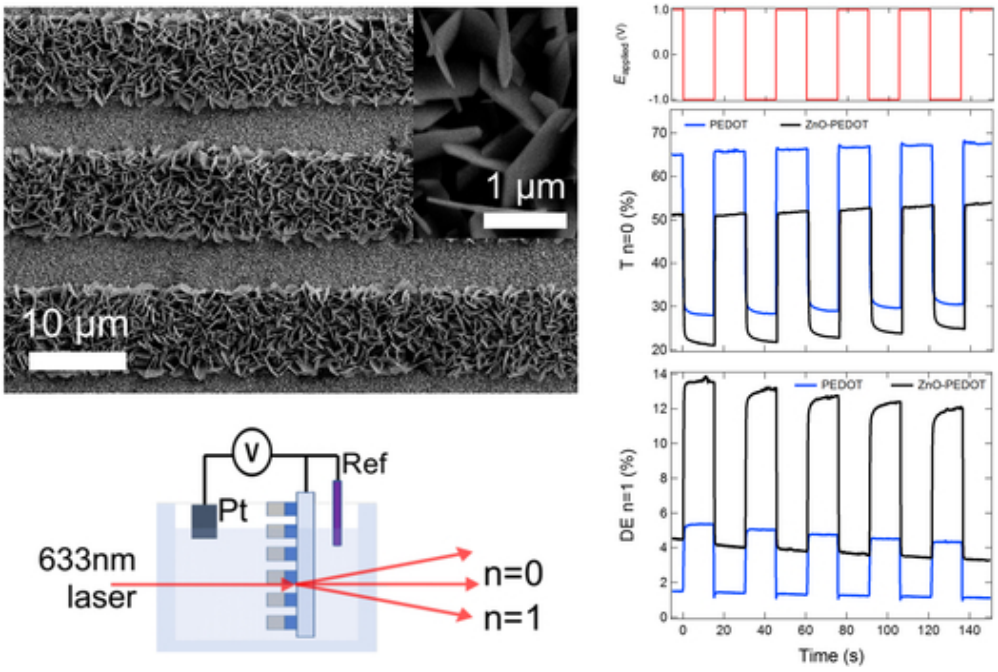

TOC Graphic

44x29mm (300 x 300 DPI)